Modeling and Simulation of Spacecraft Solar Array Deployment

B. Wie,* N. Furumoto,† A. K. Banerjee,‡ and P. M. Barba§
Ford Aerospace and Communications Corporation, Palo Alto, California

This paper presents the dynamic and digital simulation of the deployment of rigid solar panels on INTELSAT-V and INSAT spacecraft. Each spacecraft is characterized by very distinct mechanisms for its solar array deployment. The arrays on INTELSAT-V are in a topological tree configuration, while the INSAT arrays are in a closed-loop configuration because of the four-bar linkage deployment mechanism. It is shown that the kinematic control rod on the INSAT has a synchronizing function very similar to that of the closed cable loop on the INTELSAT-V spacecraft. Practical aspects of the modeling and simulation of complex deployment mechanisms are emphasized. The use and limitations of the DISCOS multibody code for deployment dynamics simulations are discussed, and the need for developing specialized simulation tools emphasized.

As spacecraft become larger and more complex, the need for stowing the spacecraft within the dimensions of the launch-vehicle fairing becomes a serious design constraint. For this reason, spacecraft are being built which are stowed in one configuration, then deployed into another configuration once in orbit. INTELSAT-V and INSAT spacecraft, shown in Figs. 1a and 1b respectively, are examples of such spacecraft, with large solar-panel arrays which must be deployed for the normal orbit configuration.

Deployment dynamics of rigid/flexible appendages for various spacecraft configurations have been investigated in the past. Practical considerations of the deployment mechanisms on the INTELSAT-V spacecraft have been discussed.[1] Some further mathematical discussions on the INTELSAT-V array deployment and a physical interpretation of its closed cable loop function will be presented in this paper. Dynamic modeling and simulation of the flexible appendage deployment can be found in Refs. 2-3.

Two different deployment mechanisms on INTELSAT-V and INSAT spacecraft will be investigated in this paper. The INTELSAT-V arrays are in a so-called topological tree configuration, while the INSAT arrays are in a closed-loop configuration because of the four-bar linkage mechanism. The closed-loop multibody configuration poses a unique dynamic problem in formulating the equations of motion.[4,5]

It will be shown that the kinematic control rod on the INSAT has a synchronizing function very similar to that of the closed cable loop on the INTELSAT-V. Practical aspects of using various simplified models will be emphasized. Some merits and drawbacks of using a general-purpose multibody code such as DISCOS[6,7] for complex deployment analyses will also be discussed. This paper addresses two major issues that arise in the modeling and simulation of complex deployment dynamics: how one can formulate analytically the complex equations of motion, and to what extent one can utilize a multibody computer code.

Received May 21, 1985; revision received Jan. 23, 1986.

*Engineering Specialist; currently at The University of Texas at Austin. Member AIAA.

†Principal Engineer; currently at Systems Control Technology Inc., Palo Alto, CA.

‡Senior Engineering Specialist; currently at Lockheed Missile & Space Company, Sunnyvale, CA.

§Principal Engineer, Systems Analysis Department. Member AIAA.

Description of Deployment Mechanisms

INTELSAT-V and INSAT spacecraft have very distinct deployment mechanisms for their solar-panel arrays. Their deployment mechanisms are also completely different from the roll-out-type mechanisms of the flexible solar arrays to be used for the future large space platform. These deployment mechanisms have dynamic characteristics similar to those encountered in the multi-joint robot arms.[8]

INTELSAT-V, shown in Fig. 1a, has two symmetric solar-panel arrays which deploy simultaneously in an accordion-type manner. These consist of a yoke and three solar panels. A schematic of the deployment mechanism consisting of torsion springs and closed cable loops is shown in Fig. 2. To prevent large disturbance torques to the mechanism, the attitude-control system is disabled during the approximately 20-s deployment period.

The preloaded torsion springs located at each hinge provide the energy to deploy the arrays, while the closed cable loops restrain the deployment by synchronizing the deployment angles. The first cable connects the first panel and the spacecraft main body, the second cable connects the second panel and the yoke, and the third cable connects the third and first panels. These cables synchronize the deployment angles of each panel by applying a "passive-control" torque which is proportional to the angle difference. Additional springs placed on the closed cables compensate for changes in cable length due to temperature variation and add considerable complexity to the mathematical model of the solar-array deployment.

The INSAT spacecraft shown in Fig. 1b has a solar array deployment sequence and mechanism quite different from the INTELSAT-V. Figure 3 illustrates the deployment sequence for the solar arrays and other appendages on the INSAT spacecraft. This deployment occurs in five separate steps, each controlled by pyrotechnic devices. As in the INTELSAT-V design, the attitude-control system is disabled during each deployment, except the solar-sail deployment. In the fully deployed configuration, the solar array is extended from the south side of the satellite, where it is oriented to the sun by the Solar Array Drive Assembly (SADA). When stowed for launch, panel 1 and the yoke are held parallel with the south wall of the satellite. Panels 2 and 4 are also folded on the south face, while panels 3 and 5 are folded against the Earth face. Two hinge assemblies are used at each of the four lines to join the panels together.

The final stage solar-array deployment of INSAT has been a major concern because of the unique dynamic characteristics of the four-bar linkage deployment mechanism. A schematic of this four-bar linkage for the final stage deployment is

shown in Fig. 4. To prevent possible interference between the array and the spacecraft main body, the control link synchronizes the deployment of the solar panel with the motion of the yoke.

It will be shown that the kinematic control rod on the INSAT has a synchronizing function very similar to that of the closed cable loop on the INTELSAT-V.

Mathematical Modeling and Digital Simulation

INTELSAT-V Solar Array Deployment

As can be seen from Fig. 2, the solar panel arrays on INTELSAT-V are in a topological-tree configuration. The solar panel itself is assumed to be rigid. It is also assumed that the solar arrays are attached to the fixed base for the deployment analysis, since the two symmetric solar arrays deploy simultaneously. As discussed before, the closed cable loops restrain the deployment by synchronizing the deployment angles. Figure 5 shows a simplified planar model with equivalent cable torques on each body.

These cable torques during the deployment are simply modeled as

$$T_1 = k(2\theta_1 - \theta_2) \tag{1a}$$

$$T_2 = k(\theta_2 - \theta_3) \tag{1b}$$

$$T_3 = k(\theta_3 - \theta_4) \tag{1c}$$

where θ_i is the ith hinge angle in unit of radians, T_i is the ith cable torque in unit of Nm, $k(=4500r^2)$ is the equivalent cable torsional stiffness in unit of Nm/rad, and $r(=1.835$ cm) is the calbe-pulley radius at panel hinges. The pulley radius at yoke hinge is $2r$, because the fully deployed yoke hinge angle θ_1 is only 90 deg while the fully deployed first panel hinge angle θ_2 becomes 180 deg.

The cable-torque model given above resembles the position-error feedback term of a conventional feedback control logic.

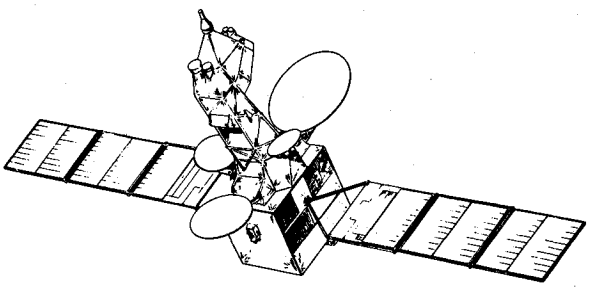

Fig. 1a INTELSAT-V on-orbit deployed configuration.

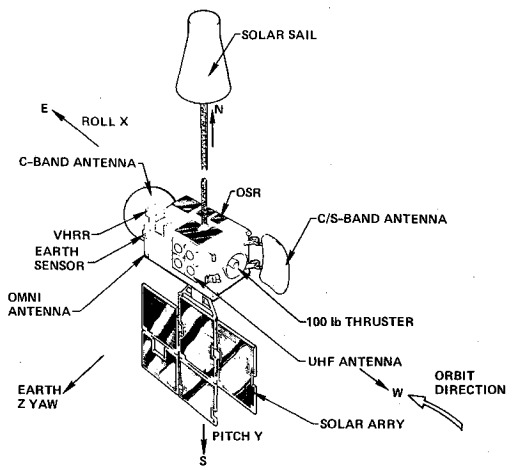

Fig. 1b INSAT on-orbit deployed configuration.

The closed cable loop applies a "passive-control" torque proportional to the angle difference in order to synchronize the deployment. The cables also serve to slow down the deployment rate to a point below the structural failure rate. In addition, springs are placed on the cables to compensate for changes in cable length due to temperature variation. In the simulations, every effort was made to implement a realistic cable-loop model. For example, after the cable springs were stretched beyond 0.72 cm, they became "hard cable," and below 0.4 cm the springs are relaxed and the cable force became zero.

It was necessary to keep the cable model simple enough so as not to have an unreasonable complexity in the simulation. The simple linear model given by Eq. (1) agrees closely with laboratory measurements to provide a sufficiently accurate description of the basic function of the closed cable loops for synchronizing the deployment.

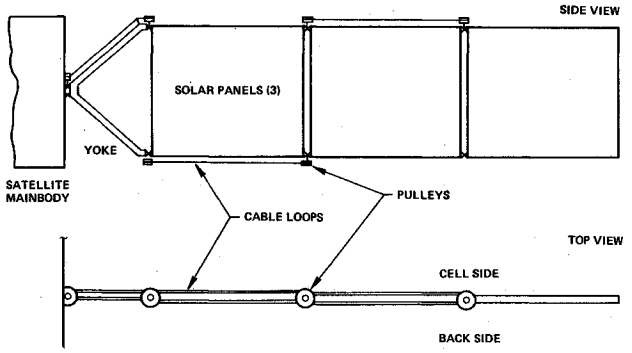

Fig. 2 INTELSAT-V solar array showing closed cable loops.

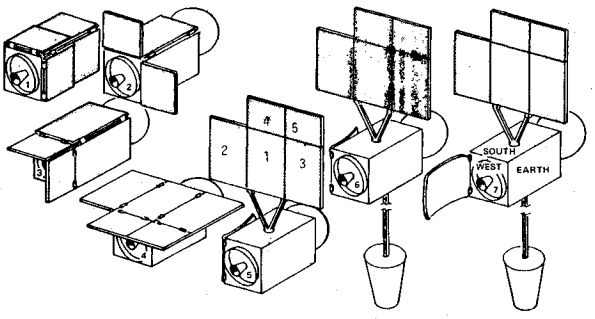

Fig. 3 INSAT deployment sequence.

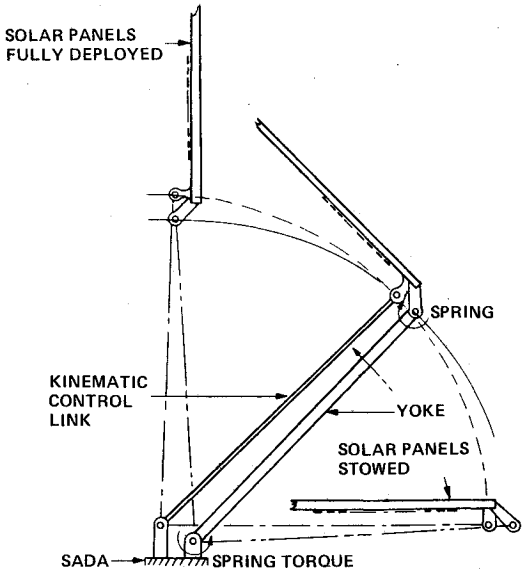

Fig. 4 INSAT array-deployment mechanism (four-bar linkage).

Table 1 INTELSAT-V solar-array deployment parameters

	Length, m	Mass, kg	Inertia, kg.m^2	Friction, Nm	Hinge spring Stiffness, Nm/rad	Hinge spring Pretorque, Nm
Yoke	1.090	2.222	0.2798	0.66	0.1273	1.70
Panel 1	1.965	12.637	4.2009	0.64	0.1305	0.85
Panel 2	1.965	9.982	3.8773	0.69	0.1305	0.85
Panel 3	1.936	8.920	2.9316	0.70	0.1305	0.85

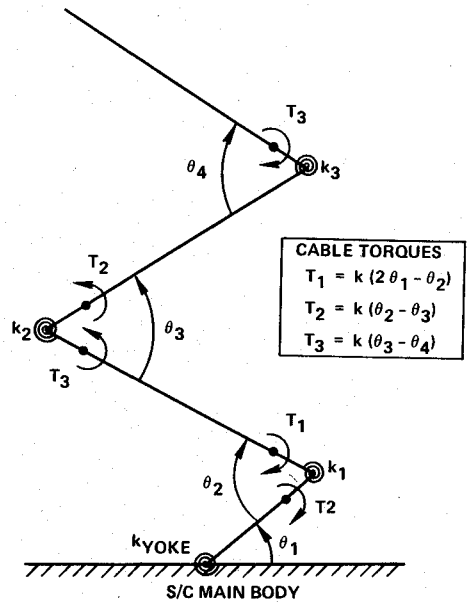

Fig. 5 INTELSAT-V array-deployment analysis model.

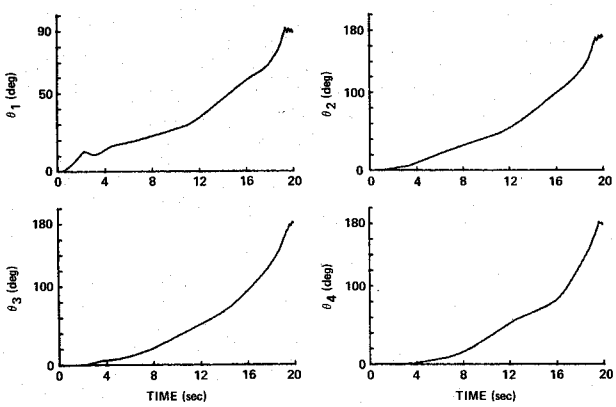

Fig. 6 Simulation results for INTELSAT-V array deployment.

The most critical parameter in the INTELSAT-V solar-array deployment is the hinge friction level, which is temperature-dependent and can be a source of premature partial deployment. Experiments have shown that the yoke-hinge friction is dependent on the angle and that the friction levels on all other hinges are virtually independent of angles. It has also been observed that there are no velocity-dependent viscous damping forces acting on the hinges. The nominal friction levels are given in Table 1 with other parameter values.

At the end of the deployment, the hinges latch into the full-deployment position. As latch-up occurs, the locking lever slides into a slot. It is assumed adequate to model the latch-up by hinges restrained by very stiff springs; however, this requires a smaller integration time step near the end of the deployment in the digital simulation. The equations of motion, written for deployment of panels from a fixed support,

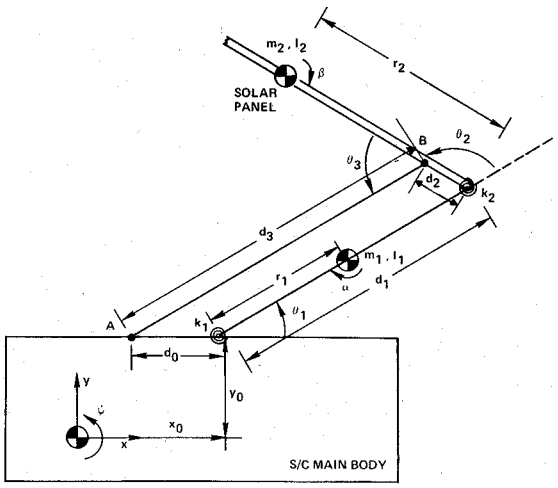

Fig. 7 INSAT array-deployment analysis model.

are represented as

$$M\ddot{\theta}+K\theta+f(\theta,\dot{\theta})=Q \tag{2}$$

where θ is the 4×1 independent generalized coordinate vector, M is the 4×4 nondiagonal time-varying mass matrix, K is the 4×4 diagonal time-invariant stiffness matrix due to the hinge springs, f is the 4×1 vector which contains nonlinear Coriolis and centrifugal forces, and Q is the 4×1 generalized force vector due to pretorque, friction, and closed cable loops. For the sake of brevity, a detailed description of each term of Eq. (2) is omitted here.

To check the simulation study results based on the above equations, a general-purpose, multibody code was introduced in the later phases of the deployment study, The INTELSAT-V array deployment problem was then studied using DISCOS (Dynamic Interaction Simulation of Controls and Structures) computer code.[6] The formulation of the equations of motion in DISCOS is based on the Lagrange method which can be used, in general, for the nonholonomic/rheonomic dynamic problems.

Figure 6 shows the simulation results using DISCOS, which exactly match the simulation results based on the analytically derived equations of motion. After the yoke initially deploys, the deployment occurs fairly evenly due to deployment synchronization by the closed cable loops.

Extensive digital simulations using both the analytically derived equations and DISCOS have been performed to investigate various effects of the hinge friction and pretorque level on the overall deployment dynamics. As a result of the digital simulations and the ground experiments, several changes to the hinges are made. Among the changes are 1) special application of lubricant to all moving parts in the hinges to reduce the hinge-friction level, 2) increase of torsion-spring pretorque level, and 3) increase of bearing tolerance to allow greater variation in temperature.

INSAT Solar-Array Deployment (Free Base and No Slot)

The analytic modeling of the INSAT final-stage deployment was not as straightforward as the INTELSAT-V case. The

four-bar linkage results in a closed-loop configuration which requires a special consideration in formulating the equations of motion, as can be seen from Fig. 4. It is also important to note that DISCOS, because of its particular formulation, introduces a constraint on a closed-loop multibody system; one member must be elastic.

To assist in the design and development of the INSAT solar-array deployment mechanisms, its dynamical behavior has been analyzed through digital simulations based on analytically derived equations. Various parameters, e.g., spring stiffness and pretorque level, linkage length, etc., were varied to determine a suitable and near-optimal set of values.

The remainder of this paper will discuss the analytical derivation of the equations and the digital simualtion results for the INSAT solar-array deployment.

A schematic of a planar simulation model is shown in Fig. 7. First, we will consider a case with a fixed base. The spacecraft is assumed to be infinitely massive and the rotational motion of the linkage and solar panel is assumed to occur about a single axis. Later we will consider a more complicated model with slotted link and coupled to the free motion of the spacecraft main body.

For the Lagrangian formulation of the equations of motion of a single model in Fig. 7, but with a fixed base, the following kinetic and potential energy terms are defined:

$$T = \tfrac{1}{2}(I_1 + m_1 r_1^2 + m_2 d_1^2)\dot{\theta}_1^2 + \tfrac{1}{2}(I_2 + m_2 r_2^2)(\dot{\theta}_1 + \dot{\theta}_2)^2 + m_2 d_1 r_2 \dot{\theta}_1(\dot{\theta}_1 + \dot{\theta}_2)\cos\theta_2 \tag{3a}$$

$$V = \tfrac{1}{2}k_1(\theta_{1F} - \theta_1)^2 + \tfrac{1}{2}k_2(\theta_2 - \theta_{2F})^2 \tag{3b}$$

where θ_{1F} and θ_{2F} are the hinge angles when the hinge springs are unstressed. The hinge angles $\theta_i (i = 1,2,3)$ and the geometrical parameters used in the above equations are defined in Fig. 7. The INSAT solar-array deployment parameters are summarized in Table 2.

Although two hinge angles are used in Eq. (3) as the generalized coordinates, they are not independent variables. Since this model has one degree of freedom, a single coordinate, such as the angle θ_2, suffices for the description of all admissible configurations. However, the kinetic energy cannot readily be expressed in terms of only θ_2 and $\dot{\theta}_2$, because of the transcendental character of the relationship among the three hinge angles. Thus the third angle θ_3 is introduced, and the angles θ_1 and θ_3 are selected as "extraneous" coordinates, which must satisfy the geometrical constraint equations

$$d_0 + d_1\cos\theta_1 + d_2\cos(\theta_1 + \theta_2) + d_3\cos(\theta_1 + \theta_2 + \theta_3) = 0 \tag{4a}$$

$$d_1\sin\theta_1 + d_2\sin(\theta_1 + \theta_2) + d_3\sin(\theta_1 + \theta_2 + \theta_3) = 0 \tag{4b}$$

Since it is impractical to isolate θ_1 and θ_3 in terms of θ_2, these holonomic-constraint equations are differentiated with respect to time and treated as nonholonomic constraints, and the dependent variables are eliminated by the method of Lagrangian multipliers.

Differentiation of the constraint equations gives

$$\dot{\theta}_1 a_{11} + \dot{\theta}_2 a_{12} + \dot{\theta}_3 a_{13} = 0 \tag{5a}$$

$$\dot{\theta}_1 a_{21} + \dot{\theta}_2 a_{22} + \dot{\theta}_3 a_{23} = 0 \tag{5b}$$

where the coefficients a_{ij} are functions of θ_1, θ_2, and θ_3. These equations are linear in $\dot{\theta}_1$ and $\dot{\theta}_3$, and they can easily be solved for these quantities in terms of $\dot{\theta}_2$.

The equations of motion can then be derived using the Lagrange multiplier method:

$$\frac{d}{dt}\frac{\partial L}{\partial \dot{\theta}_1} - \frac{\partial L}{\partial \theta_1} = \lambda_1 a_{11} + \lambda_2 a_{21} \tag{6a}$$

$$\frac{d}{dt}\frac{\partial L}{\partial \dot{\theta}_2} - \frac{\partial L}{\partial \theta_2} = \lambda_1 a_{12} + \lambda_2 a_{22} \tag{6b}$$

$$\frac{d}{dt}\frac{\partial L}{\partial \dot{\theta}_3} - \frac{\partial L}{\partial \theta_3} = 0 = \lambda_1 a_{13} + \lambda_2 a_{23} \tag{6c}$$

where $L \triangleq T - V$ is the Langrangian function and λ_1 and λ_2 are the Lagrange multipliers.

Elimination of the Lagrange multipliers in Eqs. (6), using Eqs. (5) leads to:

$$\ddot{\theta}_2 = f(\theta_i, \dot{\theta}_i) \tag{7}$$

where a detailed description of the right-hand side is given in the Appendix. Equations (5a), (5b), and (7) constitute a set of three simultaneous differential equations in the unknown functions θ_1, θ_2, and θ_3. The selection of an independent coordinate is somewhat arbitrary. Here, θ_2 has been selected as the independent coordinate to simplify the equations.

Table 2 INSAT final stage solar array deployment parameters

Spacecraft body yaw inertia I_z, kg.m^2	360.3
Yoke hinge location w.r.t. S/C body c.m., m	$(x_0, y_0) = (-0.2171, 0.7409)$
Distance d_0 from yoke hinge to control rod, m	0.15225
Yoke length d_1, m	1.32588
Distance d_2 from yoke/panel hinge to control rod, m	0.08024
Control rod length (min, max), m	$(d_{3\min}, d_{3\max}) = (1.3939, 1.4165)$
Distance r_1 from yoke hinge to yoke c.m., m	0.8915
Distance r_2 from yoke/panel hinge to panel c.m., m	1.8288
Yoke mass m_1, kg	8.899
Panel mass m_2, kg	36.891
Yoke inertia I_1 about its c.m., kg.m^2	0.9369
Panel inertia I_2 about its c.m., kg.m^2	43.527
Yoke spring constant k_1, Nm	0.6114
Yoke spring zero-torque angle θ_{1F}, deg	240
Data used for Fig. 9	
$k_2 = -0.776$ Nm/rad, 5 deg $< \theta_2 <$ 172.8 deg	
$k_2 = -40.1$ Nm/rad, -3 deg $< \theta_2 <$ 5 deg	
$\theta_{2F} = 298$ deg, 5 deg $< \theta_2 <$ 172.8 deg	
$\theta_{2F} = 12.7$ deg, -3 deg $< \theta_2 <$ 5 deg	
Initial angles θ_1, θ_2, θ_3, deg	0.294, 172.817, 7.283
Deployed yoke/body spring constant, Nm/rad	1582.3
Deployed panel/yoke spring constant, Nm/rad	28523.5
Deployed modal damping ratio	0.02
Fully deployed fixed-base frequencies, Hz	0.5, 2.74

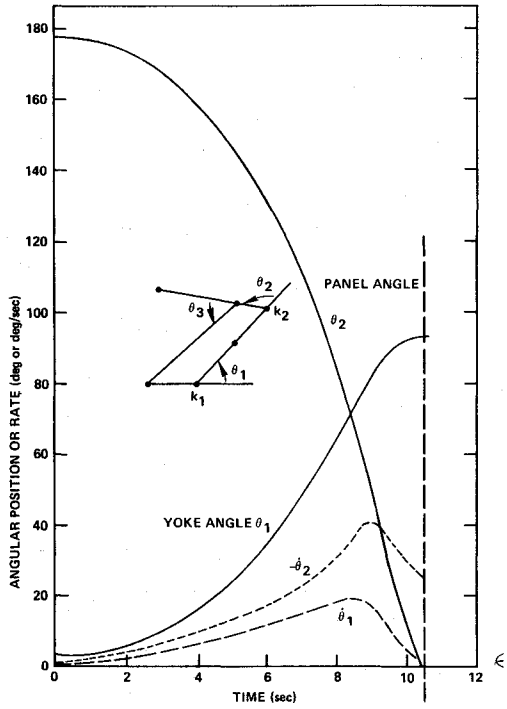

Fig. 8 Simulation results for INSAT array deployment (fixed base, no slot).

The results of the digital computer using these analytically derived equations with parameter values given in Table 2 are plotted in Fig. 8. The complete deployment takes about 10.5 s, which closely matches the actual flight-observed deployment of 11 s. Although the model used in this simulation is simple (planar, fixed based, and no slot), the simulation results provided insights into the magnitude of deployment speeds and load as a function of time and their sensitivities to various parameters of the four-bar linkage mechanism.

INSAT Solar-Array Deployment (Free Base and Slotted Link)

Since it was desired to predict the spacecraft main-body attitude motions during appendage deployment, a more complex model with a free motion of the main body was necessary. In this section, the dynamic modeling and digital simulation with a free motion of the main body will be briefly discussed. The effect of a slotted link will also be discussed. The array products of inertia were not included in this model. Array vibration after lock-up is modeled by two springs, at the yoke/body and array/yoke hinges. Spring and damping constants are tuned to give the first two fixed-based bending mode frequencies and a modal damping ratio of 0.02.

The equations of planar motion were derived using a Lagrangian approach. The kinetic energy is obtained in the form as

$$T = \tfrac{1}{2}\dot{q}^T M(q)\dot{q} \tag{8}$$

where

$$q = (x_c, y_c, \psi, \alpha, \beta)^T$$

(x_c, y_c) are the spacecraft body mass center, and (ψ, α, β) are the rotational angles of the spacecraft body, yoke, and array, respectively, relative to the inertial space. The derivation of the system kinetic energy is straightforward, assuming planar inertia distribution of the yoke and panels. There is no potential energy since the spring torques are treated as generalized forces via virtual work. The equations of motion are then

$$\frac{\mathrm{d}}{\mathrm{d}t}\frac{\partial T}{\partial \dot{q}_i} - \frac{\partial T}{\partial q_i} = Q_i + \lambda c_i \tag{9}$$

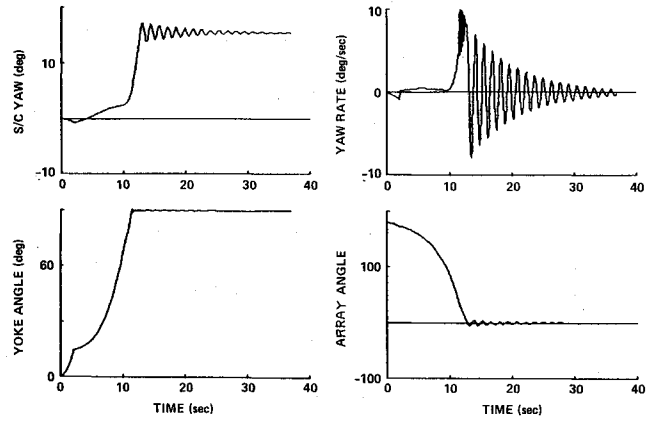

Fig. 9a Simulation results for INSAT array deployment (free base, slotted link) showing simulated spacecraft deployment behavior.

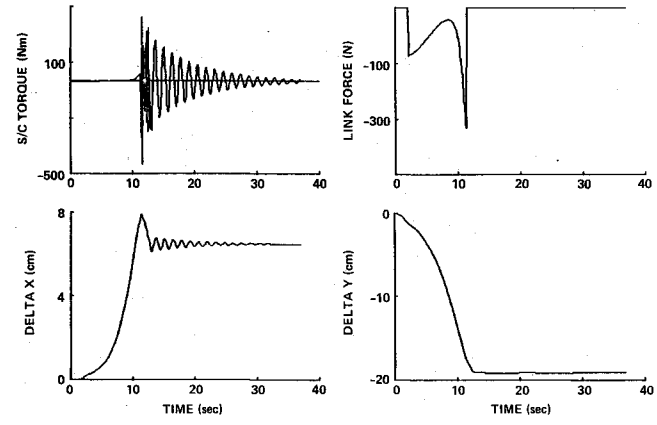

Fig. 9b Simulation results for INSAT array deployment (free base, slotted link) showing spacecraft torque, link constraint force, and (x,y) translation of main body.

The control rod is assumed to have negligible mass. It simply enforces a kinematic constraint. An inequality constraint results because the control rod is slotted at the point A in Fig. 7. If $d_3(q)$ is defined as the distance between points A and B, the control rod imposes a constraint of the form

$$d_{3\min} \le d_3(q) \le d_{3\max} \tag{10}$$

This inequality constraint is treated by means of a switching logic as follows. If the constraint is inactive, the Lagrangian multiplier is taken off and the unconstrained motion equation integrated to the next time step. If this predicts that a length bound will be hit soon, smaller time steps are taken until impact occurs. Completely plastic impact is assumed, i.e., after impact, $\dot{d}_3 = \ddot{d}_3 = 0$. This condition is enforced by calculating an impulse (directed along the rod axis) which nullifies momentum in the rod direction. When a constraint is active, the constraint equation is formed as

$$\ddot{d}_3 = \sum_{i=1}^{5} (c_i \ddot{q}_i + \dot{c}_i \dot{q}_i) = 0 \tag{11}$$

and the Lagrangian multiplier is turned on.

Equations (9) and (10) are combined to yield

$$\begin{bmatrix} M & c \\ c^T & 0 \end{bmatrix} \begin{bmatrix} \ddot{q} \\ -\lambda \end{bmatrix} = \begin{bmatrix} f(q,\dot{q}) \\ -\sum_{i=1}^{5} \dot{c}_i \dot{q}_i \end{bmatrix} \tag{12}$$

where c is a 5×1 vector with components c_i defined by Eq. (11). Thus accelerations and the link force are computed. The constraint becomes inactive when $\lambda = 0$ is found. Note that the nonlinear terms $f(q,\dot{q})$ follow entirely form Eq. (9). The nominal parameter values are given in Table 2.

Figure 9a shows the simulated spacecraft deployment behavior. It can be seen that the overall response characteristics between Figs. 8 and 9a are in good agreement, with the exception of the initial yoke response. The yoke-angle plot shows clearly the effect of impact of the slotted link. The yoke also locks up slightly before the array does. The spacecraft yaw offset is about 16 deg, with peak yaw rates up to 10 deg/s. After the yoke initially deployed, the overall deployment occurred fairly evenly. By comparing this with the INTELSAT-V yoke response in Fig. 6, it is noticed that the kinetmatic control rod on the INSAT has a synchronizing function very similar to that of the closed cable loop on the INTELSAT-V.

Figure 9b shows the spacecraft torque, the link constraint force, and the (x,y) translation of the main body. A peak compressive force of about 220 N (50 lbf) is carried by the link. This is well within the designed capacity of the link. The link effectively pushes up the panel to expedite its clearance from the spacecraft body.

Similar to the INTELSAT-V deployment analyses, a general-purpose multibody computer code was introduced in the later phases of the study. The very important problem of closed-loop configuration was pertinent in using the DISCOS computer code for the INSAT array deployment analysis. In DISCOS it is required to have an elastic member for any closed-loop configuration; it cannot directly handle a closed-loop rigid multibody system. Because of the presence of the slotted link, requiring on-off constraints with diferent constraints at the "on" states, and because of the requirement that DISCOS imposes on having flexible links, the use of DISCOS for the simulation of INSAT final array deployment was not successful. Even for a closed-loop configuration with truly elastic members, there is the problem of selecting the appropriate flexible mode shapes, e.g., Craig-Bampton modes[9] or other assumed modes.

Although the planar models discussed previously were accurate enough for the deployment-dynamics analysis of a planar linkage, some concern of the product of inertia of solar-panel array resulted in the development of a three-axis model. Because of the difficulty of using DISCOS for a closed-loop system, the three-axis coupled equations were written using Kane's approach.[5,10,11,12] Kane's method was used for the three-axis model because of its efficiency and simplicity in deriving analytical equations for very complex multibody systems (see Ref. 12 for a comparison of various analytical methods).

The simulation results using the complete three-axis coupled equations validated the use of a simplified planar model. The effect of panel product of inertia on the overall deployment behavior was found to be negligible. Details of modeling and simulation for three-axis coupled deployment dynamics are omitted here because the equations are quite unwieldy and in fact represent a rigid-body version of the equations reported in Ref. 5.

In recent years, computer programs for the automatic generation of symbolic equations of motion for complex spacecraft have been developed[12-14]. Such programs will eliminate the time-consuming part of the analytic formulation and will also automatically generate symbolic equations for more efficient simulations. However, further research is needed into practical applications of new automated modeling techniques to real complex spacecraft.

Conclusions

This paper has described two different deployment mechanisms used on the INTELSAT-V and INSAT spacecraft. Practical aspects of the dynamic modeling and simulation have been emphasized. It was shown that the kinematic control rod on the INSAT has a synchronizing function very similar to that of the closed cable loop on the INTELSAT-V. This paper has also assessed the validity of using relatively simple models, which makes it possible to analyze with confidence much more complex models in further phases of the study. The use of the DISCOS multibody computer code has shown its usefulness for simulating topological-tree dynamics.

Appendix

$$f(\theta,\dot{\theta}) = \{H[R(\dot{\theta}_1+\dot{\theta}_2)\dot{\theta}_3 + (\dot{\theta}_2+\dot{\theta}_3)\dot{\theta}_1]$$
$$\div\tan(\theta_2+\theta_3) - P\dot{\theta}_1^2\sin\theta_2 - k_2(\theta_2-\theta_{2F})(1+Q)$$
$$-P(\dot{\theta}_1+\dot{\theta}_2)^2\sin\theta_2 - k_1(\theta_1-\theta_{1F})Q\}/J_T$$

where

$$J_1 = I_1 + m_1r_1^2 + m_2d_1^2 \qquad J_2 = I_2 + m_2r_2^2$$

$$P = m_2d_1r_2 \qquad Q = [d_2\sin\theta_3]/[d_1\sin(\theta_2+\theta_3)]$$

$$R = [d_2\cos\theta_3]/[d_1\cos(\theta_2+\theta_3)]$$

$$H = [J_2 + P\cos\theta_2 - (J_1 + P\cos\theta_2)/Q]/(1+Q)$$

$$J_T = J_2 - PQ\cos\theta_2 - HQ$$

References

[1]Vorlicek, P. L., Gore, J. V., and Plescia, C. T., "Design and Analysis Considerations for Deployment Mechanisms in a Space Environment," *Proceedings of the 16th Aerospace Mechanisms Symposium*, Kennedy Space Center, FL., May 13-14, 1982, pp. 211-221.

[2]Lips, K. W. and Modi, V. K., "Three-Dimensional Response Characteristics for Spacecraft with Deploying Flexible Appendage," *Journal of Guidance and Control*, Vol. 4, Nov.-Dec. 1981, pp. 650-656.

[3]Ibrahim, A. E. and Misra, A. K., "Attitude Dynamics of a Satellite During Deployment of a Large Plate-Type Structure," *Journal of Guidance and Control*, Vol. 5, Sept.-Oct. 1982, pp. 442-447.

[4]Boland, P., Samin, J. C., and Willems, P. Y., "Stability Analysis of Interconnected Deformable Bodies with Closed-Loop Configuration," *AIAA Journal*, Vol. 13, July 1975, pp. 864-867.

[5]Banerjee, A. K. and Kane, T. R., "Large Motion Dynamics of a Spacecraft with a Closed-Loop, Articulated, Flexible Appendage," AIAA Paper 84-1015, May 1984.

[6]Bodely, C. S., Devers, A. D., Park, A. C., and Frisch, H. P., "A Digital Computer Program for the Dynamic Interaction Simulation of Controls and Structures (DISCOS)," Vols. I and II, NASA Technical Paper 1219, May 1978.

[7]Chodas, J. L. and Macala, G. A., "Validation of the Galileo Scan Platform Control Design using DISCOS," AIAA Paper 84-1964, Aug. 1984.

[8]Asada, H. and Youcef-Toumi, K., "Analysis and Design of a Direct-Drive Arm with a Five-Bar-Link Parallel Drive Mechanism," *The 1984 American Control Conference*, June 1984, pp. 1224-1230. 1224-1230.

[9]Craig, R. R. and Bampton, M. C. C., "Coupling of Substructures for Dynamic Analyses," *AIAA Journal*, Vol. 6, July 1968, pp. 1313-1319.

[10]Kane, T. R., Likins, P. W., and Levinson, D. A., *Spacecraft Dynamics*, McGraw-Hill Book Company, 1983.

[11]Kane, T. R. and Levinson, D. A., "Formulation of Equations of Motion for Complex Spacecraft," *Journal of Guidance and Control*, Vol. 3, March-April 1980, pp. 99-112.

[12]Rosenthal, D. E. and Sherman, M. A., "Symbolic Multibody Equations via Kane's Method," AIAA Paper 83-303, Aug. 1983.

[13]Macala, G. A., "SYMBOD: A Computer Program for the Automatic Generation of Symbolic Equations of Motion for Systems of Hinge-Connected Rigid Bodies," AIAA Paper 83-013, Jan. 1983.

[14]Kreuzer, E. J. and Schiehlen, W. O., "Computerized Generation of Symbolic Equations of Motion for Spacecraft," *Journal of Guidance, Control and Dynamics*, Vol. 8, March-April 1985, pp. 284-287.